Dynamic-physical model to predict the performance of a solar chimney in a warm-humid climate with different absorbent materials

Luis Godoy-Vaca[1], Manuel Almaguer[1], Juan Kastillo[1], Javier Martínez[1,2], Andrea Lobato-Cordero[1]
[1]Instituto Nacional de Eficiencia Energética y Energías Renovables, Quito, Ecuador
[2]Universidad Internacional SEK Ecuador, Quito EC170134, Quito, Ecuador
Correspondence: luis.godoy@iner.gob.ec

Abstract

The aim of this research is to simulate the performance of a solar chimney located in a warm-humid climate using a dynamic-physical model, which evaluates different absorbent materials. The model was simulated in Python programming software in order to predict the temperature distribution and the mass flow of the chimney over time. The results obtained were first compared with experimental data for dry-warm climate. Then, the model was evaluated and tested over real weather conditions. In addition, the assumed chimney dimensions were chosen according the literature for the studied conditions. In spite of evaluating the best nightly ventilation, different chimney wall materials were tested: solid brick, common brick and reinforced concrete. The results showed that, for warm and humid climate, it is better to use solid brick. It is due to the solid brick high heat capacity, which can accumulate the heat during the day and discharge during the night.

Introduction

Over the last years, energy consumption in buildings has increased due to the incorporation of heating devices, ventilating/ventilation and air conditioning (HVAC) systems in households. In fact, this energy consumption corresponds to the 40% of the total worldwide energy consumption (Wan et al. 2011). Natural cooling is a passive strategy for building conditioning. Therefore, solar chimneys are one of the potentially effective low carbon techniques. Solar chimneys use solar energy for heating or cooling buildings.

This type of systems can reduce the total fan shaft power requirements up to 50% annually, according to Shi and Zhang (2016). In order to achieve this requirement, one or more transparent wall(s) should be necessary to allow an enough heat income from the solar radiation to create the thermal buoyancy effect. As a result, an air temperature difference is created. A density gradient between the inside and outside of the chimney is obtained, which induces a natural upwards movement of air.

In pursuance of finding the optimum chimney design solutions, several mathematical and experimental studies have been carried out to enhance volume flow rate, air velocity and air temperature. These taking into account different design parameters such as: height, width, depth of cavity, chimney position, type of glazing, type of absorber and the inclusion of insulation of thermal mass.

Furthermore, the impact of air movement and temperature decrement in a solar chimney with different mathematical models are showing in Bassiouny and Koura (2008) and Shi and Zhang (2016) study. For example, Bansal et al. (2005) developed a steady-state mathematical model for a solar chimney system. It consists of a solar air heater connected to a conventional chimney, where a temperature distribution was obtained. Furthermore, Ong (2003) has presented a mathematical model of a solar chimney in steady-state using a matrix method for solving simultaneous heat transfer equations. He discretized and solved mass, momentum and energy conservation equations using the finite difference method. The author carried out an experimental study for a solar chimney to validate the proposed mathematical model.

Researches performed by Martı and Heras-Celemin (2007) related to a dynamic-physical model are applied to study the non-uniform temperatures distribution of a chimney, applied in warm-dry climates. The results were compared with a real system. Good results were obtained when testing the nocturnal ventilation by the effect of thermal inertia using reinforced concrete for the wall. On the other hand, an experimental study carried out by Arce et al. (2009) showed that in a day with maximum solar radiation, a discharge coefficient of 0.52 was obtained. This value corroborates many studies that placed this factor for warm dry climates.

Chungloo and Limmeechokchai (2007) predicted the thermal behavior of two passive cooling systems for warm-humid climates. The systems were experimentally evaluated by using a low discharge coefficient, due to the presence of humidity, to calculate the rate of air changes in several seasons of the year. Several values of solar radiation were evaluated and it was demonstrated that water should be sprayed on top of the solar chimney when the solar radiation is the highest, for there will be more air movement inside the gap.

With the purpose of implementing a solar chimney in a house of social interest in Malaysia (with warm humid climate); Pau Chung et al. (2014) engaged this passive ventilation system into a house. He calculated the thermal comfort and demonstrated that: by using a solar chimney. The average temperature inside the house decreases 2,6% while air velocity increases around 15%. This is beneficial for this type of climates. A few studies analyzed the performance of a solar chimney in hot humid climates. Sudprasert et al. (2016) performed a study testing different heights and a reduced backward flow at the opening. The yield of ventilated airflow was 15.4–26.2% less, while the overall air temperature was higher for a solar chimney with moist air.

Afonso and Oliveira (2000) studied the behavior and implications regarding a solar chimney dimensions. In addition, solid brick was used as an absorbent material for the wall. They noticed that a greater thickness had better nocturnal ventilation. Moreover, Ji et al. (2009) performed a study on a common brick wall as the ventilation system. This studies showed that both solid and common brick are widely used in the construction of solar chimneys.

Therefore, this study provides a comprehensive research on the performance of a solar chimney located in warm-humid climate considering different absorbent materials (thermal mass). To predict the air mass flow of solar chimneys under various scenarios (daytime and nighttime ventilation), a dynamic physical model was developed which was verified by using experimental data from the literature. This model was developed through an energy and mass balance analysis and it was solved using finite differences. This method was solved and simulated using programming language in Python.

Simulation

Case study

To evaluate the performance of a solar chimney in a warm climate, it is necessary to define dimensions as well as physical characteristics of the materials. The proposed dimensions correspond to studies performed in dry warm climates by Martı and Heras-Celemin (2007) since these values have been tested in several climates and they have achieved the best mas flow results.

These values will be useful to corroborate the mathematical model that will be programmed in Python. Once the dimensions of the chimney have been defined, the elements that constitute the chimney are described below:

Glass: It was assumed a glass thickness of 0.5 mm, an absorption coefficient ($\propto_g$) of 0.006; a transmissibility (τ_g) of 0.84; and an emissivity ($\in_g$) of 0.8.

Fluid: The chimney shaft width was 14.5 cm. The inlet and outlet air opening areas were 0.025 m^2.

Wall: The wall was assumed to be made of reinforced concrete, 24 cm thickness and 2 m height. The inner surface of the wall was painted black. Therefore, the assumed solar radiation absorption ($\propto_w$) was 0.82; thermal conductivity (k_w) is 1.63 W/mK; emissivity ($\in_w$) is 0.95; heat capacity (c_w) is 1090 J/KgK; and a density (ρ_w) is 2400 Kg/m^3.

In order to determine the number of intervals in which the wall is divided, the following convergence criteria is used:

$$\propto \frac{\Delta t}{\Delta x^2} < 0.25 \tag{1}$$

The model was solved only using three points with the goal of decrees the simulation time. On the other hand, the period of time used to define the minimum interval of distance between each point was one hour since weather data used for the simulation had the same interval. In this case：

$$\Delta x = 0.12 \; m \tag{2}$$

Thus, for a thermal diffusivity of the concrete which value is $\propto = 6.23 \times 10^{-7} \frac{m^2}{s}$ and $\Delta t = 3600 \; s$:

$$\propto \frac{\Delta t}{\Delta x^2} = 0.156 < 0.25 \tag{3}$$

In order to solve this equation system, it is necessary to take into consideration some aspects. Each new wall temperature depends on the temperature and heat transfer parameters at a previous time. For this case, the previous conditions for the first calculation (time 0) are not known, that is why, the wall temperatures (To=308 K, T1=307 K, T1s=303 K) are constant and equal to the conditions of Martı and Heras-Celemin (2007).

At the same way, the environmental conditions such as: temperature, solar radiation, vertical surface and wind speed; are the same as Martı and Heras-Celemin (2007) for dry and warm condition, every hour. The physical process involved in this model is presented in Figure 1.
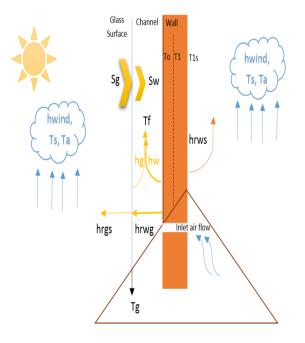

Figure 1: Physical model scheme of solar chimney.

Model

The mathematical concepts that were used as baseline for creating this software are detailed in Martı and Heras-Celemin (2007). The solar chimney model was developed using the programming language python as shown by

Palach (2014) in its version 3.4. The class design follows the Object Oriented Programming paradig.

The multiple mathematical operations, that are performed following the model, were developed using the parallel programming tools of Python, which has many advantages as shown by Palach (2014). In order to speed up the final result, it was used the Python multiprocessing package, which allows to perform concurrent operations on Cpython's Global Interpreter Lock (GIL). It also allows to exploit all the cores of the computer, which cannot be achieved using the threading package Friborg (2009). All the processes created shared a common queue, provided by the multiprocessing package, where they write the obtained results.

Variable Configuration

Before starting the simulation process it is necessary to configure the variables to be used in the software. Even though the solar chimney's default values are used, the variables that are part of the the solar chimney can be customized. The main variables are the properties of the wall, weather and glass.

The weather data to be used in the simulation can be read from EPW files as well as from any plain text file in CSV format. It should be noted that, for CSV formatted text files, the position of each of the weather variables must be specified. EPW files contain one year of weather data. It can take a lot of time to simulate a whole year, the software allows to specify the range of time to do the simulations.

First Simulation Phase

The first phase of the simulation consists of finding the values of the following variables: Fluid Temperature (Tf), Glass Temperature (Tg) and Temperature of the Wall that connects to the duct (To). For this, a range of variation is established for each of these variables and the increment for the variation is done in decimals. For each value, the calculation of the *approximation* (4) to 0 is performed by the following equation,

$$approx = Sg + (Hg * (Tf - Tg)) + (Hrwg * (To - Tg)) - (hwind * (Tg - Ta)) - (Hrgs * (Tg - Ts)). \qquad (4)$$

The primary objective is to find an approximation value as close as possible to 0. This calculation is performed by processes implemented in Python simultaneously. When a process finishes, it is responsible for writing in the queue the best approximation value obtained and the combination of the variables To, Tg, Tf used to obtain the result. To carry out this operation, it is necessary to previously perform operations that solve the value of the variables involved in the equation, among which are *Sg* (5), *Hrwg* (6), *Hrgs* (7) and *Hg* (8), which are shown below,

$$Sg = \alpha g * Rad. \qquad (5)$$

$$Hrwg = \sigma * (((Tg^2 + To^2) * (Tg + To)) / ((1 / Eg) + (1 / Ew) - 1)) \qquad (6)$$

$$Hrgs = (\sigma * Eg) * (Tg + Ts) * (Tg^2 + Ts^2) \qquad (7)$$

$$Hg = Nuga * kga / Lw. \qquad (8)$$

For the calculation of *Hrwg* (6) and *Hrgs* (7), it is necessary to use of the *SteffanBoltzmann* constant (σ), which has a value of 5.67×10^{-8} W·m^{-2}·K^{-4}. The calculation of the variable *Hg* (8) has dependence on variables that must be solved before being able to complete this calculation.

First, the *kga* (9) variable can be solved as it follows,

$$kga = 0.0263 + (0.000074 * (tmga - 300)). \qquad (9)$$

The *Nuga* (10) value depends on the value that the *Raga* (13) variable takes, if *Raga* (13) is less than 10^9, then the following formula will be used for its calculation,

$$Nuga = 0.68 + (0.67 * Raga^{(1/4)}) / (1 + (0.492 / Prga)^{(9/16)})^{(4/9)}. \qquad (10)$$

Otherwise, the *Nuga* (11) value will be calculated as it follows,

$$Nuga = 0.68 + (0.67 * Raga^{(1/4)}) / (1 + (0.492 / Prga)^{(9/16)})^{(4/9)}. \qquad (11)$$

Despite the previously used scenario, it is necessary to make use of the variables *Raga* (13) and *Prga* (12), which are calculated according to the following formulas,

$$Prga = ufga * Cpga / kga \qquad (12)$$

$$Raga = Prga * grga \qquad (13)$$

The calculation of *Prga* (12) and *Raga* (13) variables introduces new variables *grga* (14), *ufga* (15), *Cpga* (16) and *kga* (17), they must be solved as follows,

$$grga = (9.8 * \beta ga * \Delta ga * (Lw^3)) / (vfga^2) \qquad (14)$$

$$ufga = (1.846 + (0.00472 * (tmga - 300))) * 10^{-5} \qquad (15)$$

$$Cpga = (1.007 + (0.00004 * (tmga - 300))) * 10^3 \qquad (16)$$

$$kga = 0.0263 + (0.000074 * (tmga - 300)). \qquad (17)$$

In turn *grga* (14) needs βga (18), Δga (19) and *vfga* (20),

$$\beta ga = 1 / tmga \qquad (18)$$

$$\Delta ga = |Tg - Tf| \qquad (19)$$

$$vfga = ufga / pga \qquad (20)$$

Where the variables $tmga$ (21) and pga (22) are calculated as follows,

$$tmga = (Tg + Tf) / 2 \qquad (21)$$

$$pga = 1.1614 - (0.00353 * (tmga - 300)). \qquad (22)$$

All the calculations detailed above aim to find the approximate value closest to 0, which will be used in the second phase of the simulation together with the variables Sw (23), Hw (25) and pwa (26), which must still be calculated using the following formulas,

$$Sw = \tau g * \alpha w * Rad \qquad (23)$$

$$pwa = 1.1614 - (0.00353 * (tmwa - 300)) \qquad (24)$$

$$Hw = (Nuwa * kwa) / Lw \qquad (25)$$

$$kwa = 0.0263 + (0.000074 * (tmwa - 300)). \qquad (26)$$

The $Nuwa$ (27) value depends on the value of the variable $Rawa$ (30), if $Rawa$ (30) is less than 10^9, then the following formula will be used for its calculation,

$$Nuwa = 0.68 + (0.67 * Rawa^{(1/4)}) / (1 + (0.492 \qquad (27)$$
$$/ Prwa)^{(9/16)})^{(4/8)}.$$

Otherwise the $Nuwa$ value will be calculated using the following formula,

$$Nuwa = (0.825 + (0.387 * (Rawa^{(1/6)})) / (1 + \qquad (28)$$
$$(0.492 / Prwa)^{(9/16)})^{8/27})^2$$

Whatever the scenario used previously, it is necessary to make use of the variables $Prwa$ (29) and $Rawa$ (30), which are calculated according to the following formulas,

$$Prwa = (ufwa * cpwa) / kwa \qquad (29)$$

$$Rawa = Prwa * grwa. \qquad (30)$$

For the calculation of the variables $Prwa$ (29) and $Rawa$ (30), new variables such as $cpwa$ (31), $ufwa$ (32) and $grwa$ (33) must be obtained and they must be solved as it follows,

$$cpwa = (1.007 + (0.00004 * (tmwa - 300))) * \qquad (31)$$
$$10^3$$

$$ufwa = (1.846 + (0.00472 * (tmwa - 300))) * \qquad (32)$$
$$10^{-5}$$

$$grwa = (9.8 * \beta wa * \Delta wa * (Lw^3)) / (vfwa^2). \qquad (33)$$

In the previous formulas, new variables $tmwa$ (34), βwa (35), Δwa (36) and $vfwa$ (37) are introduced and they must be calculated by the following formulas,

$$tmwa = (Tf + To) / 2 \qquad (34)$$

$$\beta wa = 1/tmwa \qquad (35)$$

$$\Delta wa = abs(To - Tf) \qquad (36)$$

$$vfwa = ufwa / pwa. \qquad (37)$$

Each created process implements the calculations detailed above. All the necessary variables are obtained in order to continue the simulation process. The results of each process are written in a queue for further processing. Once all the processes have been completed, the best result obtained from each process is written in a new queue and sorted by their proximity to 0, regardless of whether they are positive or negative.

Mass flow

The mass flow is calculated out of the best values obtained in the previous process. In cases where $Tf - Ta$ is less than 0, the mass flow is assigned the value of 0. Otherwise its calculation is done by the following formula,

$$massFlow = Cd * ((pwa * Aow) / \qquad (38)$$
$$\sqrt{(1 + Aow/Aiw)} *$$
$$\sqrt{((2 * g * Lw * (Tf - Ta)) / Ta)}).$$

Programming conditions

The best-obtained values are analyzed. Some defined rules are applied with the objective of selecting the best value amongst all. The rules developed for this version of the software are hard coded. It is expected that the next version of the software will include capabilities for configuring and adjusting the rules per the preferences of each user. Each applied condition is weighted with a value. In case that a condition is fulfilled, the weights are added. Sorting in descending order based on the sum of the fulfillment of each condition allows to have in the first place the value that more rules has fulfilled.

The conditions were defined taking into consideration the opinion of field experts that are members of the project. To use an example, one of the applied rule is related to the Ta value, in case the Ta value undergoes a decrease, both the values of Tg and Tf are expected to decrease too. This series of conditionals helps the solar chimney in

maintaining a logical and, to some extent, a predictable behavior within the expected parameters.

Second Phase of the Simulation

First thing to do for the second phase of the simulation is to find the next value of the *To* variable. To accomplish this, the chimney wall has been divided into three points: *To*, *T1s* which is the midpoint of the wall and *T1* which is the inner end of the wall. To represent the temperatures over time, the same variable is used and 1 is added at the end, so that *To* at the next instance of time is represented by *To1*, *T1s* at the next instance of time is represented by *T1s1* and *T1* is known by *T11*. The formulas used in the second phase of the simulation are shown below.

$$To1 = ((Sw - (Hw * (To - Tf)) - (Hrwg * (To - Tg)) - ((Kfw / \Delta x) * (To - T1))) * ((2 * 3600) / (Cw * Pw * \Delta x))) + To \quad (39)$$

$$T11 = (((\alpha * 3600) / \Delta x^2) * (T1s + To - (2 * T1))) + T1 \quad (40)$$

$$T1s1 = ((((Kfw / \Delta x) * (T1 - T1s)) - (hwind * (T1s - Ta)) - (Hrws * (T1s - Ts))) * ((2 * 3600) / (Pw * Cw * \Delta x))) + T1s \quad (41)$$

$$Hrws = (0.0000000567 * Ew) * (T1s + Ts) * (T1s^2 + Ts^2) \quad (42)$$

Once the variables *To*, *T1s*, *T1* have been solved in the next instance of time, the variables *Tg* and *Tf* are calculated. This time it is not necessary to vary *To* since it has already been resolved.

After the processes responsible for varying *Tg* and *Tf* are created, it begins a loop where all the operations described from the first phase of the simulation until now are repeated. The loop runs as many times as is specified in the variable configuration, where the time period defines the number of iterations performed by the software. Each result obtained from the iterations is stored in a list, which is finally persisted to a plain text file.

Validation

After finishing the Python program, the obtained graphs were used to validate the dynamic physical model proposed by Martı and Heras-Celemin (2007) as shown in figures 2-5. During daytime the ambient temperature is higher than the glass temperature as is showed in Figure 2. The opposite occurs at night, where the ambient temperature decreases. Consequently, at a certain time, the ambient temperature less or the same than the glass temperature.
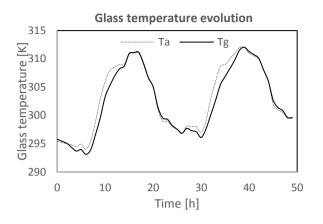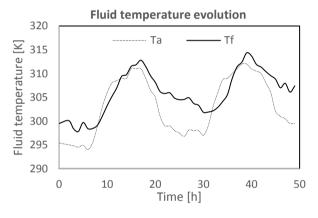

Figure 2: Glass temperature evolution.

The fluid temperature is higher than the ambient temperature in most of the time (Figure 3), except for a few hours in where the ambient temperature and solar radiation are increasing.
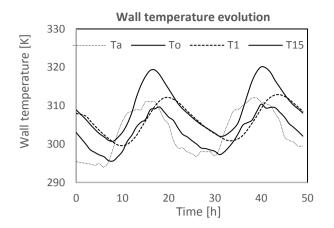

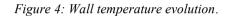*Figure 3: Fluid temperature evolution.*

In Figure 4 shows the temperature difference between the inner surface of the concrete wall and outer temperature reaches 9 K at midnight. It indicates that in the night hours the wall has thermal inertia. The air volume that crosses the chimney are presented in figure 5. It reaches its maximum value at 22:00 h. The volume air flow is superior to 0.010 Kg/s during most of the time of simulation, even at the same hours at Martı and Heras-Celemin (2007) when they are nil around 11 am. These results allow the validation of the mathematical model.
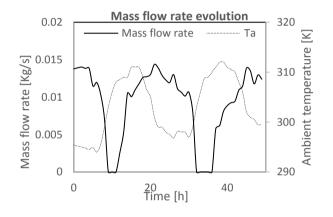
Figure 4: Wall temperature evolution.

Figure 5: Mass flow that crosses the chimney.

Once that the obtained results were very close to the studied ones, it is possible to enter into the Python program a climatic file that should contain: solar radiation, ambient temperature and wind speed, as well as constructive aspects and properties of the materials, to obtain the distribution of temperatures and mass flow over time.

Discussion and results analysis

A real weather data series from a meteorological station, corresponding to two days of measurements: October 16th and 17th, 2015 have been used. These days were selected where the incident solar radiation was complete with clear sky conditions. Data was recorded in IKIAM University, Tena, Ecuador (warm-humid zone). The data of the two consecutive days correspond to constant and highest values of solar radiation and environmental temperature. Furthermore, the measured wind speed was the lowest and relative humidity registered the lowest values at noon. This data was hourly recorded and represented in figure 6.
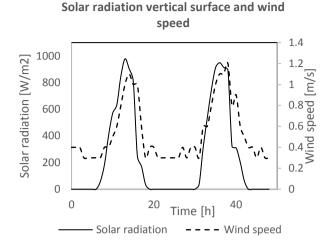

Figure 6: Weather real data, corresponding to two days in Tena, Ecuador.

From the results presented by Sudprasert et al. (2016), where the presence of moist air for chimney applications in warm humid climates was analyzed, the same dimensions of the chimney were collected for the current analysis. With these values and climatic data in Tena, Ecuador, the different materials were tested in the software. The materials properties are shown in Table 1. In this work, three types of materials were analyzed, the most frequently used in the construction of solar chimney walls.

Table 1: Material properties evaluated for the wall of the chimney.

Wall material	Thermal conductivity, Kw (W/mk)	Heat capacity, Cw (J/KgK)	Density, ρ (Kg/m^3)
Reinforced Concrete, C	1.63	1090	2400
Solid brick, SB	0.87	1330	1800
Common brick, CB	0.87	840	1800

As shown by Afonso and Oliveira (2000), a higher thickness of the wall allows to storage more energy in the wall by decreasing the flow rate during sunshine hours and increasing it during the night period. A higher thickness is better for night ventilation. Generally, a brick wall thickness is 12 or 24 cm. The highest value was considered for these calculations.
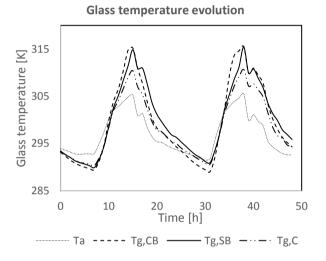
The configuration considered was west orientated, vertical chimney, since the highest the solar radiation occurred in the afternoon and because the chimney is located near the equator. On the other hand, fabrication costs for vertical configurations are lower than costs for inclined configurations.

Results analysis

Glass temperature evolution

As shown in Figure 7, the temperatures of the glass were higher than the ambient temperatures compared to the temperatures recorded in dry hot climates. It is due, of the high solar radiation in this zone. Also, it is important to note that the common brick reached the highest value of temperature more rapid than the other materials, when ambient temperature increased. The same effect took place with the temperature decreasing in the afternoon. On the other hand, solid brick temperature reached almost the same temperature as the common brick, but slowly. Besides the solid brick temperature decreased the slowest until it reached the same temperature value of the concrete when the walls were totally discharged.

Glass temperature evolution

Fig. 7. Results of evolution of the glass temperatures with different materials.

Fluid temperature evolution

Something similar to the glass temperature evolution occurred with the fluid temperature evolution as shown in figure 8. Most of the time, fluid temperature inside solid brick wall shaft was greater than the temperature when using the other materials. The fluid temperature using solid brick reached its highest value at the 15th and 38th hour after the measurement started. It coincides with the highest ambient temperatures recorded as well.
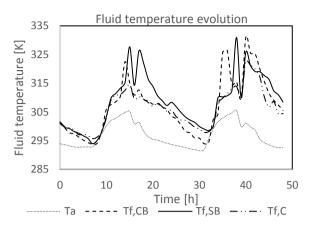
Fluid temperature evolution

Figure 8: Results of evolution of the fluid temperature with different materials.

Wall temperature evolution

Wall temperature inside the chimney made of common brick was higher at same higher radiation value; but decreases rapidly, compared to solid brick and reinforced concrete. Although, the reached value of the temperatures, when the higher solar radiation happens, were different for all materials. At the lowest value, both solid brick temperature and reinforced concrete temperature became the same. On the other hand, common brick temperature decreased quickly and reached a lower value at the 8th and 32th hours, as shown in figures 9-a, 9-b and 9-c.
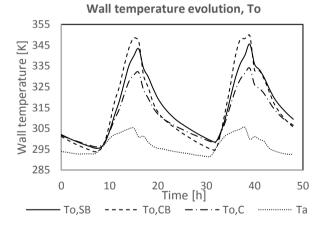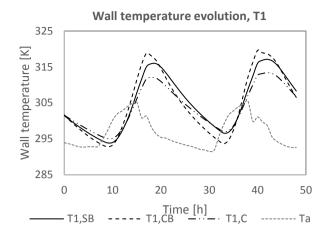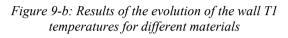
Wall temperature evolution, To

Figure 9-a: Results of the evolution of the wall To temperatures for different materials.

BUILDING
SIMULATION 2017

INTERNATIONAL
BUILDING
PERFORMANCE
SIMULATION
ASSOCIATION

Figure 9-b: Results of the evolution of the wall T1 temperatures for different materials
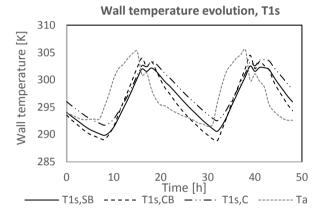

Figure 9-c: Results of the evolution of the wall T1s temperatures for different materials

Mass flow rate evolution

Figure 10 shows the value of solid brick mass flow, compared to other materials was higher most of the time. In addition, it can be observed that the mass flow, when analyzing the common brick, is 0 at the hours 8 and 32.
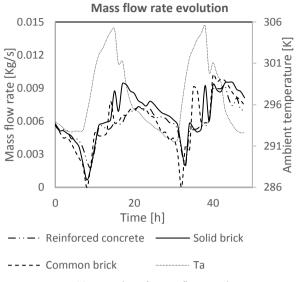

Figure 10: Results of mass flow evolution temperatures with different materials.

Discussion

The proposed dynamic physical model was validated. It showed consistent results that were similar to the studies carried out by Martí and Heras-Celemin (2007). This mathematical model was programmed in Python in order to obtain glass, fluid and wall temperature evolution and the mass flow evolution. The input variables to the program were: climatic data, dimensions of the chimney and properties of different construction materials.

In order to observe the behavior of the solar chimney in warm humid climates, the input data for the program was real weather data of Tena, Ecuador. This zone has particular weather conditions for example, the wind speed is lower than the zones near to the ocean. These factors determined the importance of a solar chimney for a house, because the chimney allows not only to decrease the temperature inside the house as well as the relativity humidity rate. The chimney also, create greater airflow changes that lead to a healthier ambient. Another important variable in this zone to take into account was moist air, which is why, as the work of Sudprasert et al. (2016) showed. For this weather condition, a solar chimney should have specific dimensions (3 m high and 0.2 m channel width) to improve the chimney performance.

Another important parameter is the wall material that will perform as heat accumulator. According to literature, it is important the highest temperature inside the shaft. This improve the thermic buoyancy effect and thus, to obtain a bigger mass rate that reduces the vapor mass attached to the hot weather air. In addition, accurate material picking for the insulating wall causes a thermal inertia positive effect that improves nighttime ventilation. Several studies tested different wall materials for the chimney. Based on a bibliographic compilation three materials for the chimney walls were chosen for testing: reinforced concrete, common brick and solid brick. The wall width

BUILDING
SIMULATION 2017

INTERNATIONAL
BUILDING
PERFORMANCE
SIMULATION
ASSOCIATION

was 24 cm, the most used value for solar chimneys (Martı and Heras-Celemin 2007) and (Afonso and Oliveira 2000).

Once that the required input data such as: environmental conditions, dimensions and materials characteristics was provided; the program showed the profile temperature and flow mass versus time functions for each analyzed material. In each graph it was observed that the highest temperature was reached for common brick. This is because common brick's heat capacity is the lowest of all material's, as is its thermal conductivity. It allows to concentrate the heat on the wall surface, but not to let it inside the material too fast. It causes that the heat can be released rapidly, promoting a low nighttime ventilation.

On the other hand, the reinforced concrete had the lowest temperature distribution. It is due, of its high thermal conductivity and medium heath capacity. It did not produce a high increment in temperature, but it let the heat to release slowly. This material even reached the same temperature of solid brick, when the heat has been totally released, at 8 am. Nevertheless, the solid brick showed a medium temperature compared to the other materials, despite the fact that it takes more time for the material to increase its temperature (compared to common brick), and the heat is released more slowly. With all of this facts in mind, it is recommendable for this type of climate, to use solid brick as insulating material since it reaches higher temperatures, than reinforced concrete. In addition, the heat is released more slowly than in common brick. This results were reflected in the mass flow rates obtained, where the air flow rate in a solid brick chimney is often higher than flows in other materials.

In a study carried out by Pau Chung et al. (2014), it was possible to see a highest mass flow velocity value with a solar chimney was recorded at 6 pm. Similar results has been exposed in this work. Furthermore, a higher temperature inside the chimney shaft is beneficial for the studied climate. It is due, to the humidity that reduces the fluid velocity in 15.4 – 25.2 % compared to dry climates (Sudprasert 2016). This work showed a good comparison between different chimney wall materials for hot-moist climates.

Conclusions

This study is used to define the best wall material for a solar chimney placed in a warm-humid climate, by considering the variations on weather conditions such as: solar radiation, relative humidity and ambient temperature; as well as construction aspects. The chimney performance was evaluated through the analysis of local air velocity distribution and temperature distribution.

The obtained results in the present study permitted to observe the best material performance and thus, to recommend the use of solid brick as a wall material in a solar chimney. Because of solid brick's high heat capacity, it can absorb and accumulate heat. It is beneficial at night, when heat is discharged. In fact, the heat absorbed during the day is not transferred to the house. This material could be used at the same time as heat absorbing material and as insulating material.

References

Afonso, C., & Oliveira, A. (2000). Solar chimneys: simulation and experiment. *Energy and Buildings*, *32*(1), 71-79.

Amori, K. E., & Mohammed, S. W. (2012). Experimental and numerical studies of solar chimney for natural ventilation in Iraq. *Energy and Buildings*, *47*, 450-457.

Arce, J., Jimenez, M. J., Guzman, J. D., Heras, M. R., Alvarez, G., & Xamán, J. (2009). Experimental study for natural ventilation on a solar chimney. *Renewable Energy*, *34*(12), 2928-2934.

Bansal, N. K., Mathur, J., Mathur, S., & Jain, M. (2005). Modeling of window-sized solar chimneys for ventilation. *Building and Environment*, *40*(10), 1302-1308.

Bassiouny, R., & Koura, N. S. (2008). An analytical and numerical study of solar chimney use for room natural ventilation. *Energy and buildings*, *40*(5), 865-873.

Chungloo, S., & Limmeechokchai, B. (2007). Application of passive cooling systems in the hot and humid climate: The case study of solar chimney and wetted roof in Thailand. *Building and Environment*, *42*(9), 3341-3351.

Friborg, R. M., Bjondalen, J. M., & Vinter, B. (2009, November). Three Unique Implementations of Processes for PyCSP. *In CPA*. 277-292.

Hirunlabh, J., Kongduang, W., Namprakai, P., & Khedari, J. (1999). Study of natural ventilation of houses by a metallic solar wall under tropical climate. *Renewable Energy*, *18*(1), 109-119.

Ji, J., Luo, C., Sun, W., Yu, H., He, W., & Pei, G. (2009). An improved approach for the application of Trombe wall system to building construction with selective thermo-insulation façades. *Chinese Science Bulletin*, *54*(11), 1949-1956.

Lutz, M. (2014). Python pocket reference. *O'Reilly Media, Inc*. 1- 266.

Martı, J., & Heras-Celemin, M. R. (2007). Dynamic physical model for a solar chimney. *Solar Energy*, *81*(5), 614-622.

Ong, K. S. (2003). A mathematical model of a solar chimney. *Renewable Energy*, *28*(7), 1047-1060.

Palach, J. (2014). Parallel Programming with Python. *Packt Publishing Ltd.*1-106.

Pau Chung, L, Mohd Hamdan Ahmad & Dilshan Remaz Ossen. (2014, August). Implementation of Solar Chimney in Orang Asli Settlement in Bukit Lagong,

Selayang. Paper presented at *5th International Graduate Conference on Engineering Science & Humanity*.

Shi, L., & Zhang, G. (2016). An empirical model to predict the performance of typical solar chimneys considering both room and cavity configurations. *Building and environment, 103*, 250-261.

Sudprasert, S., Chinsorranant, C., & Rattanadecho, P. (2016). Numerical study of vertical solar chimneys with moist air in a hot and humid climate. *International Journal of Heat and Mass Transfer, 102*, 645-656.

Wan, K. K., Li, D. H., Liu, D., & Lam, J. C. (2011). Future trends of building heating and cooling loads and energy consumption in different climates. *Building and Environment, 46*(1), 223-234.

Nomenclature

Hg	transfer coefficient between glass and air
Hrgs	transfer coefficient between the glass and the sky
Hrwg	transfer coefficient between wall and glass
Hrws	transfer coefficient between wall and the sky
Hw	transfer coefficient between wall and air
Sg	solar radiation gain by the glass
Sw	solar radiation gain by the wall
Tf	fluid temperature
Tg	glass temperature
To	outlet wall fluid temperature
βwa	coefficient of expansion of wall-air
kwa	conductivity of the concrete wall
cpwa	specific heat wall-air
Δwa	difference temperature wall-air
pwa	density wall-air
grwa	Rayleigh number for the surface wall-air
Nuwa	Nusselt number for the surface wall-air
Prwa	Prandtl number wall-air
Rawa	Rayleigh number for the surface wall-air
tmwa	mean temperature wall-air
ufwa	wall-air viscosity
βga	coefficient of expansion of glass-air
kga	thermal conductivity glass-air
Cpga	specific heat glass-air
Δga	difference temperature glass-air
grga	Rayleigh number for the surface glass-air
Nuga	nusselt number for the surface glass-air
Prga	Prandtl number glass-air
Raga	Rayleigh number for the surface glass-air
tmga	mean temperature glass-air
ufga	viscosity glass-air
αg	absorptivity of glass
Eg	emissivity of the glass
τg	transmissivity of glass
Aiw	area of the inlet of the chimney
αw	wall absorptivity
Aow	area of the outlet of the chimney
Cw	wall specific heat
Pw	wall density
α	thermal diffusivity
Ew	emissivity of the wall
Δx	distance between nodes of the concrete wall
Kfw	thermal conductivity of the concrete wall
Lw	height of solar chimney
Cd	coefficient of discharge of air channel
Rad	solar radiation on vertical surface
T1	inlet wall fluid temperature
Ta	ambient temperature
Ts	sky temperature
g	gravitational constant
hwind	Convective wind heat loss coefficient
T1s	middle wall fluid temperature
approx	approximate value to 0